# Magneto-optical effects in composite hyperbolic metamaterials

© I.V. Malysheva, S.V. Sotnichuk, A.P. Leontiev, K.S. Napolskii, I.A. Kolmychek

Moscow State University,
Moscow, Russia

E-mail: malysheva.iv@shg.ru

The results of experiments on measuring the magneto-optical response of hyperbolic metamaterials based on nanorods containing segments of gold and nickel are presented. A comparative analysis of the spectral behavior of the magnetic contrast in the geometry of Voigt and Faraday for samples was carried out, and a phenomenological description of phenomena was proposed.

**Keywords:** magneto-optical effects, plasmons, metamaterials.

## 1. Introduction

At present, the optics of nanostructures and metamaterials is a rapidly developing field of science. In particular, it is of interest to study the properties of hyperbolic metamaterials (HMMs), i.e. strongly anisotropic structures in which the components of the dielectric and/or magnetic permeability tensor have different signs [1–5]. In such media, the implementation of the hyperbolic dispersion regime is possible, as well as the appearance of the pole of the effective permittivity, Epsilon-Near-Pole (ENP), and the spectral region, where there is a sign change of the real part of the permittivity tensor component when it passes through zero value, Epsilon-Near Zero (ENZ) [1–5]. In the spectral vicinity of these points, giant birefringence, enhancement of second harmonic (SH) generation, negative refraction, enhancement of spontaneous emission, and many other interesting optical and nonlinear optical effects are observed [6–10]. The use of these structures is possible to create functional elements of nanophotonics [6], biosensors [11] and waveguides [12]. The addition of a ferromagnetic material to the composition of the HMMs leads to increase in the magneto-optical effects in the vicinity of ENZ and ENP, and therefore can expand the possibilities of controlling light parameters [13,14]. HMMs based on noble and magnetic metals combine plasmonic and magnetic properties, as well as the possibility of implementing the hyperbolic dispersion regime, which is promising for various applications.

The work is devoted to the study and comparison of the magneto-optical properties of various configurations of magnetic HMMs based on arrays of metal nanorods containing gold and nickel segments in the anodic aluminum oxide dielectric matrix.

## 2. Manufacturing and certification of structures

The formation of arrays of segmented nanorods was carried out by the method of successive template elec-trodeposition of Au and Ni into porous matrices of anodic aluminum oxide (AAO). To prepare AAO templates, high-purity aluminum foil (99.99%) was subjected to anodic oxidation at 0.3 M $H_2C_2O_4$ at 40 V by the two-stage method, the electrolyte temperature was 0°C. The thickness of the formed porous oxide layer is 35 $\mu$m. The removal of aluminum remaining after anodization was carried out by dissolving it in a mixture containing $Br_2$ and $CH_3OH$ in volume ratio of 1 : 10. Chemical etching of the barrier layer and subsequent etching of pores up to 30 nm was carried out in a 3 M solution of $H_3PO_4$ using electrochemical detection of the moment of pore opening. To create a conductive contact, the layer of gold 240 nm thick was deposited on the lower side of the templates using magnetron sputtering of Au (99.99%) target.

The electrodeposition of Au and Ni segments was performed at room temperature in three-electrode cell using a platinum auxiliary electrode. Silver chloride reference electrode was used, immersed in a saturated KCl solution, connected to the cell through a Luggin–Haber capillary. The electrodeposition of gold segments was carried out using the commercial electrolyte „Ecomet 04-3G" at potential of $E_d = -1.0$ V. Nickel was deposited using the electrolyte containing 0.6Ṁ $NiSO_4$, 0.1Ṁ $NiCl_2$, and 0.3Ṁ $H_3BO_3$, the deposition potential was $E_d = -0.9$ V. To increase the nucleation rate, the pulse $E_{imp} = -1.2$ V (for Au) or $E_{imp} = -1.1$ V (for Ni) with duration of 0.1 s was applied before metal deposition. The charge density spent on the deposition of gold and nickel was 50 mC/cm² and 18 mC/cm², respectively, in the case of two-segment nanorods. For HMMs of Au/Ni/Au composition, similar values were 36 mC/cm² and 15 mC/cm². When calculating the charge density, normalization was carried out on the geometric area of samples.

The analysis of the SEM images for the cleavages of the obtained composites indicates the uniform filling of the matrix channels with metals (Fig. 1, *a*). For a sample based on two-segment rods, the length of the gold segments
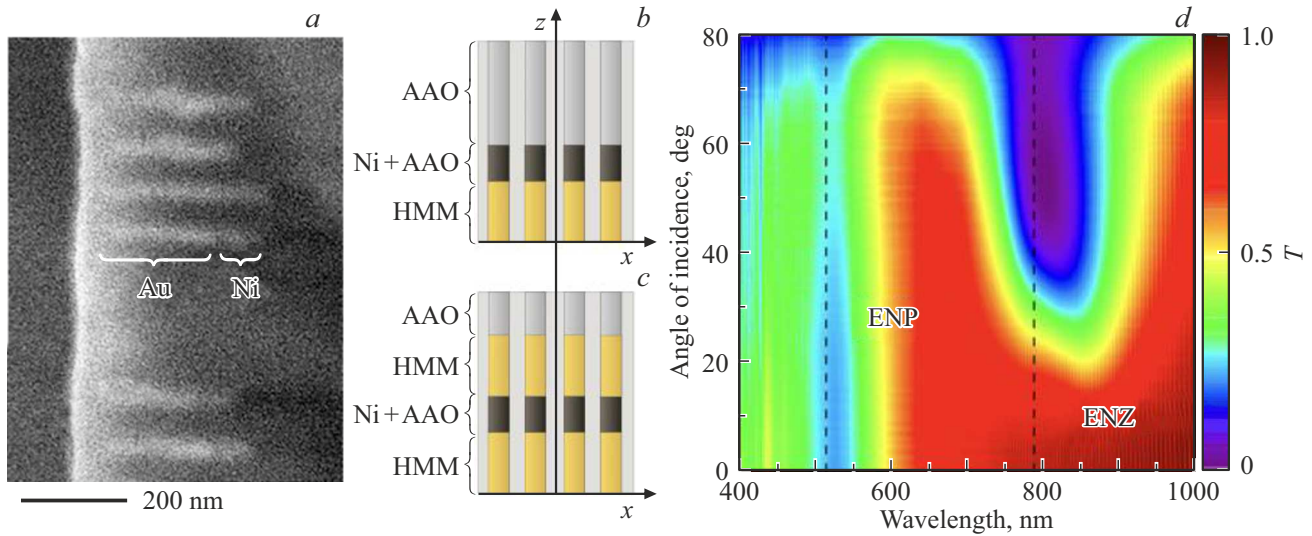
**Figure 1.** $a$ — SEM image of a HMM cleavage based on two-segment nanorods; $b, c$ — schemes of the structures under study; $d$ — frequency-angular transmission coefficient spectrum of HMMs based on two-segment Au/Ni nanorods.

are $188 \pm 8$ nm, the nickel segments are $70 \pm 3$ nm, the diameter is $27 \pm 6$ nm (diagram in Fig. 1, $b$). For HMM structures of gold–nickel–gold composition, the total length of nanorods is $220 \pm 23$ nm, the length of nickel segments is $18 \pm 3$ nm, and the diameter is $30 \pm 5$ nm (the diagram in Fig. 1, $c$). Gold is needed to excite high-quality plasmon resonances, and nickel is needed to observe magneto-optical effects [12]. Before optical measurements, the lower layer of the current collector was removed in argon plasma.

Figure 1, $d$ shows the frequency-angular spectrum for transmission coefficient of HMMs based on Au/Ni nanorods, which demonstrates the presence of two minima. The first of them is observed in the spectral vicinity of the wavelength $\lambda = 520$ nm and is associated with the excitation of transverse (with respect to the long axis of the nanorods) plasmon resonance, the second is located at $\lambda = 780$ nm and is associated with the excitation longitudinal plasmon in nanorods. It should be noted that local surface plasmons excited in the direction parallel to the nanorod axes are not observed at normal incidence or $s$-polarization of probing radiation. For HMMs of Au/Ni/Au composition, the frequency-angle spectrum is qualitatively similar to that shown in Fig. 1, $d$, however, the long-wavelength minimum is located at the wavelength $\lambda = 645$ nm, which is associated with a larger volume fraction of metal and shorter length of nanorods. The width of the long-wavelength resonance is about $50$ nm.

## 3. Calculation of optical properties of hyperbolic metamaterials

The calculation of the components of the effective permittivity tensor for the HMMs was performed within the framework of the Maxwell–Garnett model for anisotropic medium [1]. Array of two-segment nanorods in the simplest

approximation can be represented as a sequence of three layers: an anisotropic HMM based on gold nanorods in an AAO matrix, an array of nickel segments in the same matrix, and a porous AAO layer without metal (Fig. 1, $b$). Using the permittivities of gold, nickel, and aluminum oxide, as well as the volume fraction of the metal, one can calculate the effective $\varepsilon_\perp$ and $\varepsilon_\parallel$ corresponding to the perpendicular and parallel directions with respect to the long axes of the nanorods, and at the same time determine the spectral region where the hyperbolic dispersion regime is realized in the first layer containing the Au segments. The calculation shows that the zero and pole of the effective permittivity are located near the wavelengths $780$ and $520$ nm, respectively, and the hyperbolic regime is observed at $\lambda > 780$ nm (Fig. 2, $a$). Thus, the spectral positions of the transverse and longitudinal local surface plasmons correspond to the ENP and ENZ points, respectively.

HMMs are highly anisotropic structures in which the optical axis is directed along the axis of the nanorods. The refraction indices for ordinary ($n_o$) and extraordinary ($n_e$) waves are expressed as the angle of incidence of the probing radiation on the structure $\theta$, as well as $\varepsilon_\perp$ and $\varepsilon_\parallel$:

$$n_o = \sqrt{\varepsilon_\perp}, \qquad (1)$$

$$n_e = \sqrt{\varepsilon_\perp + \sin^2\theta(1 - \varepsilon_\perp/\varepsilon_\parallel)}. \qquad (2)$$

The frequency-angular spectra of the calculated values $\mathrm{Re}(n_e)$ and $\mathrm{Im}(n_e)$ are shown in Fig. 2, $b, c$. In the spectral vicinity of ENZ, a significant modulation of $n_e$ is observed, while the absolute variation in both the real and imaginary parts of it exceeds $4$. In this case, $\mathrm{Re}(n_o) \approx 2$ over the entire spectral range under study, while $\mathrm{Im}(n_o)$ has only a small maximum in the spectral vicinity of ENP. Thus, the largest difference $\mathrm{Re}(n_e - n_o)$ is observed in the vicinity of ENZ at $\theta \approx 60°$ and reaches $3$, which is by orders of
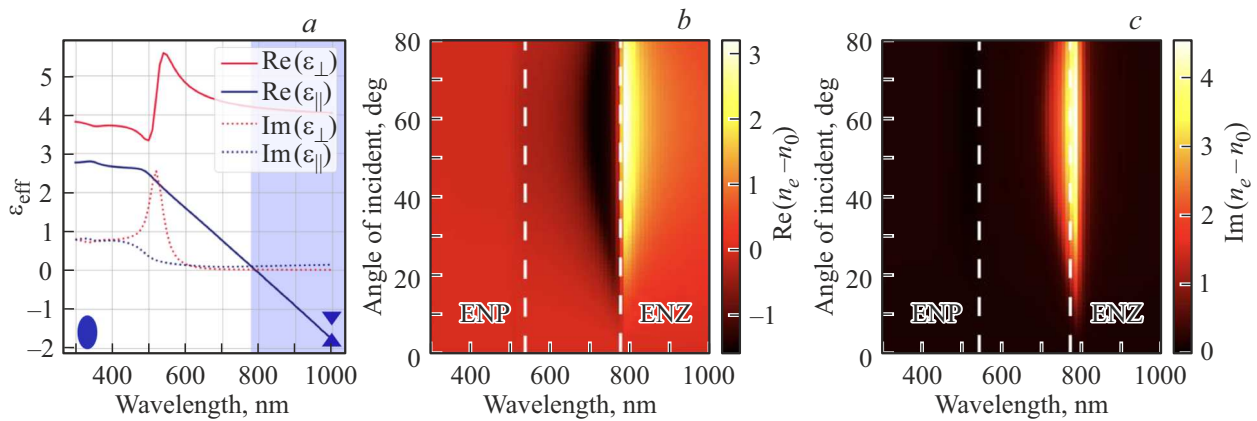
**Figure 2.** *a* are spectra of the components of the effective permittivity tensor of HMMs based on gold nanorods calculated within the framework of the effective medium model; frequency-angular spectrum of the real (*b*) and imaginary (*c*) parts of the difference between the refractive indices of the extraordinary and ordinary waves.

magnitude more than in such natural anisotropic materials like calcite or quartz in the optical range [15]. In transition from the elliptic to the hyperbolic dispersion law the sign change of $\mathrm{Re}(n_e - n_o)$ is also observed. Similarly, within the framework of the Maxwell–Garnett model for describing the properties of the second layer containing Ni segments, it is shown that the magnitudes characterizing the effect of birefringence, $\mathrm{Re}(n_e - n_o)$ and $\mathrm{Im}(n_e - n_o)$, are by three orders less than in the layer with gold segments. Thus, the structure can be represented in the form of successive layers of birefringent HMM and almost isotropic magnetic layer.

For array of Au/Ni/Au nanorods, the effective medium model is inapplicable due to the small length of the nanorod segments compared to the wavelength of the incident light (a structure of similar design with longer gold segments is practically nontransparent, which complicates studies). However, it can be assumed that the physical mechanisms of the interaction of light with the composite are similar to those observed in an array of two-segment nanorods. Then the points ENP and ENZ are at wavelengths in the region of 520 nm and 650 nm, where, according to the transmission spectrum, excitation of plasmon resonances is observed. Thus, the hyperbolic dispersion regime is reached at $\lambda > 650$ nm.

## 4. Experimental methods and results

Magneto-optical measurements were carried out on an experimental facility, where a halogen lamp was used as the source of broadband *p*-polarized light. The studied samples were placed between two magnet poles, which created the constant saturating magnetic field $H = 3$ kOe. To reveal the magneto-optical response of composites, the magnetic contrast was measured in the geometry „for transmission" over a wide incidence angle range, defined as

$$\rho = \big(T_+(\lambda, \theta) - T_-(\lambda, \theta)\big) / \big(T_+(\lambda, \theta) + T_-(\lambda, \theta)\big),$$

where $T_\pm(\lambda, \theta)$ are the transmittance factors for the opposite positions of the magnet. In the Faraday geometry, the intensity of light passing through the analyzer installed at an angle of 45° relative to the polarization of the probing radiation was recorded. In the Vocht geometry, the total intensity of the light transmitted through the sample was detected. All measurements were carried out for two orientations of the structure: when the radiation incidents from the side of the nanorods and from the side of the unfilled part of the template.

The results of magneto-optical measurements are shown in Fig. 3. For HMMs based on two-segment nanorods in the Faraday geometry, near ENZ ($\lambda = 780$ nm), an increase in the magnetic contrast is observed, as well as a change in its sign. In the case when light first falls on the layer with Ni and AAO nanosegments, and then passes into the HMM layer (Fig. 3, *a*), the magnetic contrast reaches an absolute value of 0.3% at $\theta \approx 60°$. For the opposite orientation of the sample, the amplification $\rho$ is approximately two times less (Fig. 3, *b*).

For HMMs based on three-segment nanorods of Au/Ni/Au composition, the qualitatively identical magneto-optical response is observed for both sample orientations (Fig. 3, *c*). Its maximum absolute value is reached in the vicinity of ENZ ($\lambda \sim 650$ nm) at $\theta \approx 50°$ and is 1.5% when radiation is incident from the side of the substrate and 0.4% when light is incident from the side of nanorods.

In the Vocht geometry for both types of samples, qualitatively identical frequency-angle magnetic contrast spectra are observed, which do not change when the structures are rotated by 180° (Fig. 3, *d, e*). There is an increase in the absolute value of $\rho$ and a change in its sign in the spectral neighborhood of ENZ. For arrays of two-segment nanorods at $\theta \approx 55°$, the value of magnetic contrast reaches 0.5%, while for HMMs based on Au/Ni/Au the maximum value $\rho$ is 0.2% at $\theta \approx 50°$. In the vicinity of ENP, no spectral features of the magneto-optical response upon transverse magnetization were found.
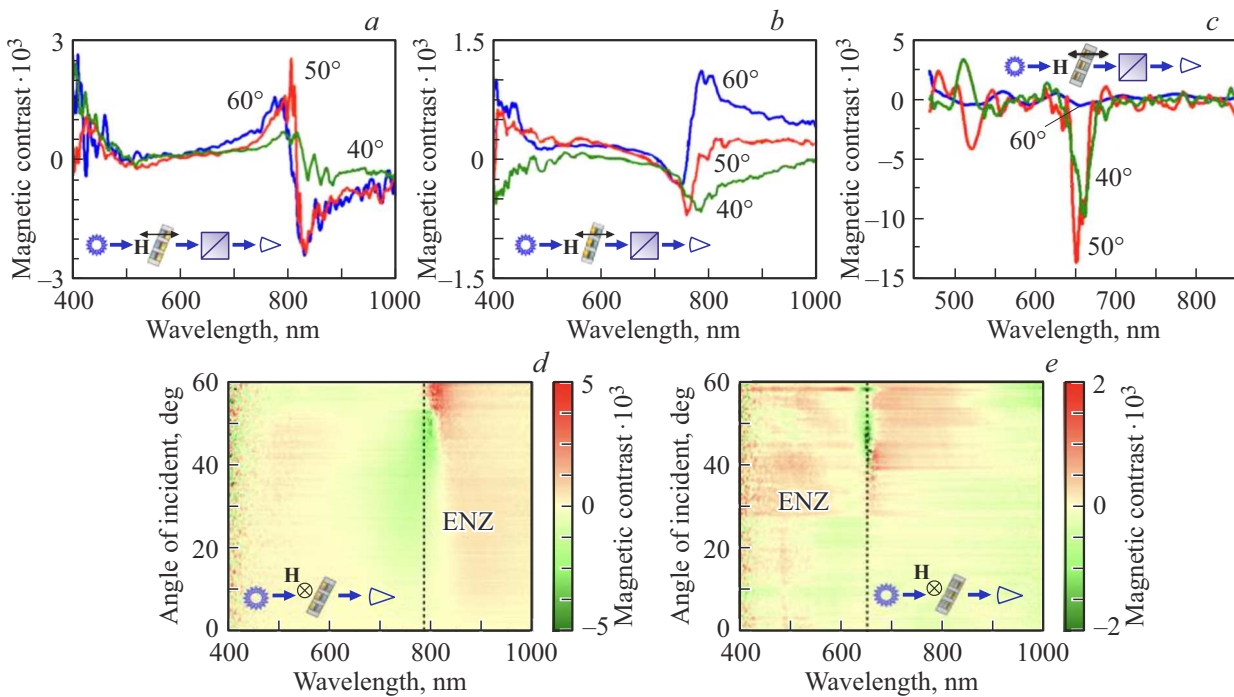
**Figure 3.** Magnetic contrast spectra: *a* — Faraday geometry, Au/Ni nanorods, light is incident from the side of gold segments; *b* — Faraday geometry, Au/Ni nanorods, light is incident from the side of nickel segments; *c* — Faraday geometry, Au/Ni/Au nanorods; *d* — Vocht geometry, Au/Ni nanorods; *e* — Vocht geometry, Au/Ni/Au nanorods. On the panels (*a−c*), angles of light incidence on the structure are indicated.

## 5. Discussion of results

The magnetic contrast modulation in the Faraday geometry corresponds qualitatively to the variation in the angle of rotation of the polarization plane in the HMMs, however, it does not make it possible to unambiguously draw a conclusion about its value, since the transmitted light acquires ellipticity due to the high anisotropy of the HMMs [6,16].

Recall that an array of two-segment nanorods can be represented as two successive layers, i.e. isotropic magnetic one and anisotropic HMM (Fig. 1, *b*). Then, in the Faraday geometry, if *p*-polarized light is incident on the structure from the side of the nickel segments, the polarization plane rotates due to the nickel gyrotropy. Thus, two waves propagate in the HMM layer: ordinary one and extraordinary one, and strong birefringence in the HMM near ENZ leads to an increase in the angle of rotation of the polarization plane. The change in the sign of the magnetic contrast in the vicinity of ENZ (Fig. 3, *a*) is due to the fact that the difference $\mathrm{Re}(n_e - n_o)$ changes sign at this point (Fig. 2, *b*).

When radiation is incident on an array of Au/Ni nanorods from the side of gold segments (Fig. 3, *b*), the mechanism of formation of the magneto-optical response in the geometry of the Faraday effect is probably as follows. When only extraordinary (*p*-polarized) wave is incident on the HMM, the polarization plane does not rotate. However, the light is partially reflected from the boundary with a layer of nickel nanosegments, and according to the calculations performed

using the data shown in Fig. 2, the Brewster angle for such an interface is about 30°, i.e., at $\theta$ in the range of approximately 40−60° the reflection of *p*-polarized light is large. When reflected from the magnetic layer, the plane of polarization rotates due to the magneto-optical Kerr effect, and then both waves, both ordinary one and extraordinary one, penetrate into the HMM layer. The layer of gold nanorods final rotates the polarization plane due to strong anisotropy, and this is most pronounced in the vicinity of ENZ. Thus, due to multiple re-reflections from the boundaries of the nanocomposite layers, the enhancement and sign change for the magnetic contrast of the light transmitted through the structure are observed.

As for the Faraday effect in an array of three-segment nanorods, then, of course, the effects of birefringence, which are observed in an array of two-segment nanorods, also play an important role in them. In this case, since the structure is symmetric, the qualitative form of the magnetic contrast spectra when radiation is incident from the side of the substrate and from the side of the nanorods is the same. To compare the magnitude of the Faraday rotation in arrays of two- and three-segment nanorods, ellipsometry data for the optical radiation transmitted through both types of samples are needed, which will probably be the subject of further research.

In the Vocht geometry, the total intensity of the light transmitted through the structure is detected, so birefringence does not play a role. In non-resonant structures, the

effect is related to the asymmetry of the boundaries of the magnetic film [16]. The main mechanism of magneto-optical response amplification and change in the sign $\rho(\lambda, \theta)$ in the vicinity of ENZ in the Vocht geometry in Au/Ni and Au/Ni/Au structures (Fig. 3, $d, e$) lies in the fact that during transverse magnetization, a magnetically induced variation in the refraction index of nickel occurs, which is odd in the magnetic field. It leads to variations in the boundary conditions at the ends of the gold nanosegments and, consequently, to a spectral shift of the longitudinal plasmon resonance. The maximum value of the magnetic contrast in array of two-segment nanorods is greater than in array of three-segment ones, since in the first case the boundaries of nickel segments are much more asymmetric (on one side there is gold, and on the other side there is air). It should be noted that the effect of the magnetically induced shift of the spectral position of the plasmon resonance can also play a role in the formation of the magneto-optical response in the Faraday geometry (Fig. 3, $a-c$).

## 6.  Conclusion

In this work, the optical properties of hyperbolic meta-materials based on arrays of nanorods consisting of Au and Ni segments in a matrix of anode aluminum oxide have been studied. The spectroscopy of magneto-optical effects in structures containing a two-dimensional hexagonal array of two-segment (Au/Ni) and three-segment (Au/Ni/Au) nanorods at different angles of incidence in a wide wavelength range, which includes special dispersion points ENP and ENZ, is performed. Enhancement of the Faraday effect in the spectral vicinity of zero effective permittivity and a change in the sign of the magnetic contrast (in the spectral vicinity of ENZ) are found. Presumably, the observed features of the magneto-optical response are associated with strong birefringence due to the hyperbolic dispersion law. In the Vocht geometry, the enhancement and sign change of the magnetic contrast in the vicinity of ENZ point occur due to the magnetically induced variation in the refraction index of nickel and the corresponding spectral shift of the resonant frequency of plasmons excited along the gold nanosegments.

### Conflict of interest

The authors declare that they have no conflict of interest.

## References

[1]  A. Poddubny, I. Iorsh, P. Belov, Y. Kivshar. Nature Photonics **7**, 948 (2013).

[2]  M.G. Silveirinha. Phys. Rev. E **86**, 046612 (2006).

[3]  N.M. Litchinitser, V.M. Shalaev. Laser Phys. Lett. **5**, *6*, 411 (2008).

[4]  V.P. Drachev, W. Cai, U. Chettiar, H.K. Yuan, A.K. Sarychev, A.V. Kildishev, G. Klimeck, V.M. Shalaev. Laser Phys. Lett. **3**, 1 (2006).

[5]  L. Ferrari, Ch. Wu, D. Lepage, X. Zhang, Zh. Liu. Prog. Quantum Electron. **40**, 1 (2015).

[6]  I.A. Kolmychek, A.R. Pomozov, V.B. Novikov, A.P. Leontiev, K.S. Napolskii, T.V. Murzina. Opt. Express **27**, 32069 (2019).

[7]  P. Ginzburg, F.G. Rodriguez Fortuno, G.A. Wurtz, W. Dickson, A. Murphy, F. Morgan, R.J. Pollard, I. Iorsh, A. Atrashchenko, P.A. Belov, Y.S. Kivsha, A. Nevet, G. Ankonina, M. Orenstein, A.V. Zayats. Opt. Express **21**, 14907 (2013).

[8]  I.A. Kolmychek, I.V. Malysheva, V.B. Novikov, A.P. Leontiev, K.S. Napolskii, T.V. Murzina. Phys. Rev. B **102**, 241405 (2020).

[9]  S. Wicharn, S. Plaipichita, Th. Seesanb, P. Buranasiri. Proc. SPIE **10516**, 105161M (2018).

[10]  I.A. Kolmychek, V.B. Novikov, I.V. Malysheva, A.P. Leontiev, K.S. Napolskii, T.V. Murzina. Opt. Lett. **45**, *7*, 1866 (2020).

[11]  A.V. Kabashin, P. Evans, S. Pastkovsky, W. Hendren, G.A. Wurtz, R. Atkinson, R. Pollard, V.A. Podolskiy, A.V. Zayats. Nature Mater. **8**, 867 (2009).

[12]  N. Vasilantonakis, M.E. Nasir, W. Dickson, G.A. Wurtz, A.V. Zayats. Laser Photon. Rev. **9**, 345 (2015).

[13]  I.A. Kolmychek, A.N. Shaimanov, A.V. Baryshev, T.V. Murzina. Pis'ma v ZhETF **102**, *1*, 50 (2015) (in Russian).

[14]  I.V. Malysheva, I.A. Kolmychek, A.M. Romashkina, A.P. Leontiev, K.S. Napolskii, T.V. Murzina. Nanotechnology **32**, 305710 (2021).

[15]  G. Ghosh. Opt. Commun. **163**, 95 (1999).

[16]  A.K. Zvezdin, V.A. Kotov. Magnitooptika tonkikh plenok. Nauka, M. (1988). 191 p. (in Russian).